

# Electric-field control of a hydrogenic donor's spin in a semiconductor

A. De, Craig E. Pryor, and Michael E. Flatté

Department of Physics and Astronomy and Optical Science and Technology Center,  
University of Iowa, Iowa City, Iowa 52242

(Dated: February 10, 2022)

An AC electric field applied to a donor-bound electron in a semiconductor modulates the orbital character of its wave function, which affects the electron's spin dynamics via the spin-orbit interaction. Numerical calculations of the spin dynamics of a hydrogenic donor (Si) embedded in GaAs, using a real-space multi-band  $\mathbf{k} \cdot \mathbf{p}$  formalism, show the high symmetry of the hydrogenic donor state results in strongly nonlinear dependences of the electronic  $g$  tensor on applied fields. A nontrivial consequence is that the most rapid Rabi oscillations occur for electric fields modulated at a *subharmonic* of the Larmor frequency.

Electronic ground states characterized by non-zero spin are attractive candidates for encoding quantum information in a solid state system, and the use of electric fields is an attractive method to address individual spins[1, 2]. When the ground state has a nonzero *integer* spin it is possible to perform all needed spin operations using electric fields alone[3, 4], whereas for manipulation of spin-1/2 electronic ground states at least a static applied magnetic field is required. Advances in focused ion beam single-ion implantation[5], as well as the use of a scanning tunneling microscope to implant a single ion with atom-scale precision[6, 7], suggest that spin clusters and spin-based circuits consisting of large numbers of precisely positioned spins could be designed with near-atomic resolution. Proposals to control individual spin-1/2 states in such an environment with local electric fields include changing the magnitude of the Landé  $g$  tensor to bring spins into resonance with an extended AC magnetic field[8, 9, 10, 11], moving spins in a fringe-field[12] or a hyperfine[13] gradient, modulating zero-field spin splittings[14, 15], and  $g$ -tensor modulation resonance ( $g$ -TMR)[16].  $g$ -TMR uses the electric-field dependence of the Landé  $g$  tensor *anisotropy* to manipulate the spin, and so does not require microwave magnetic fields or nanoscale magnetic materials or nuclear polarization gradients. Although  $g$ -TMR works by changing the orbital character of the wave function with an electric field, and thereby indirectly influencing the spin through the spin-orbit interaction, it does not require zero-field spin splittings (so  $g$ -TMR could be performed in a silicon or diamond host). Predictions for quantum dots indicate control of the  $g$  tensor anisotropy can produce rapid Rabi oscillations and full Bloch-sphere control with a single vertical electric field[17].

The promising approach of  $g$ -TMR has yet to be explored for electrons bound to dopants. Shallow donors might seem a poor candidate for modulation of  $g$  tensor anisotropy, as they have cubically-symmetric  $g$  tensors in the absence of an electric field. Quantum dots, by contrast, have highly asymmetric  $g$  tensors that are very sensitive to applied electric fields[17]. However, we find the  $g$  tensors of electronic spins bound to donors de-

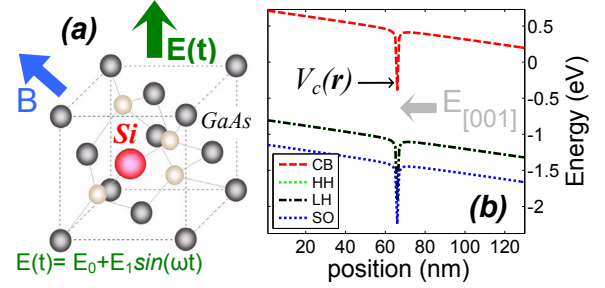


**FIG. 1** (a) Proposed geometry for  $g$ -tensor modulation. (b) The impurity potential is a Coulomb potential plus a central cell correction. The effect of applying an electric field on the zone center band energies is shown.

pend nonlinearly on applied electric and magnetic fields, and thus substantial  $g$  tensor anisotropy and rapid spin manipulation can be achieved for a hydrogenic donor state. As the dominant electric-field dependence is nonlinear, the most rapid Rabi oscillations are found at unexpected frequencies — subharmonics of the Larmor frequency rather than the fundamental — permitting rapid spin manipulation using AC electric fields with frequencies far below the Larmor frequency. Furthermore, the  $g$  tensors of quantum dots are very sensitive to dot shape and composition[18] and thus each quantum dot will have different resonance frequencies for  $g$ -TMR. Donor wave functions and  $g$  tensors will, however, each be reliably the same.

These hydrogenic states have other attractive features for spin clusters or spin devices; they possess the biggest radii of any ionic bound states in the solid, with Bohr radii of the order of 10 nm in GaAs. Thus the spin-spin coupling between states would be easier to control than for deep levels whose interaction strength changes substantially on the atomic scale[7]. Our treatment focuses on the substitutional silicon donor in gallium arsenide,  $\text{Si}_{\text{Ga}}$ , as it is one of the best understood semiconductor point defects and is well described by the hydrogenic model. We expect that similar results are possible for a shallow donor in silicon, although the details may be

complicated by the presence of multiple valleys in the conduction band.

The geometry of  $g$ -TMR for a single electron spin bound to a donor is shown in Fig. 1(a). A static magnetic field along with a gated time varying electric field is applied to the crystal containing the  $\text{Si}_{\text{Ga}}$  donor. We considered all orientations of the field and found that the most rapid Rabi oscillations occur when the magnetic field is applied at an angle  $\theta = 45^\circ$  to the electric field, which is the configuration shown in Fig. 1(a).

Although many properties of shallow impurities (such as the energy spectrum) can be treated to an excellent approximation by two-band effective mass theory[19],  $g$ -tensor calculations require a multi-band treatment as the coupling among multiple bands needs to be considered, and the spin-orbit interaction must be treated accurately[20]. Moreover, the electric field breaks the spherical symmetry of the impurity site. These complexities are best handled numerically.

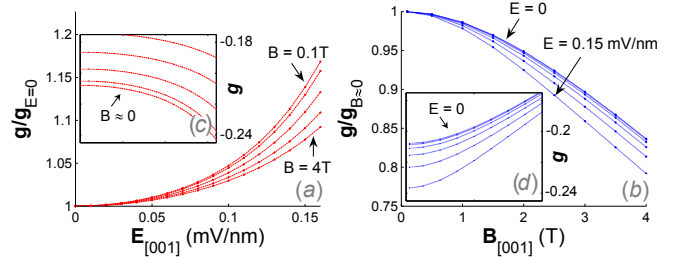
Our calculations of  $g$ -TMR for  $\text{Si}_{\text{Ga}}$  donors were carried out using 8-band  $\mathbf{k} \cdot \mathbf{p}$  theory[21] in the envelope approximation using finite differences on a real space grid [18, 22, 23, 24]. Material parameters were taken from Ref. 25 assuming  $T = 0$ . The potential of the hydrogenic impurity,

$$V_c(\mathbf{r}) = \frac{e^2}{4\pi\epsilon r} + C\delta(\mathbf{r} - \mathbf{r}_0), \quad (1)$$

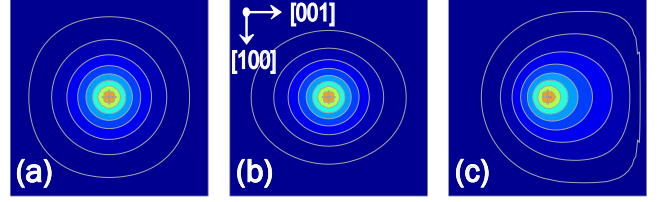
is the sum of a screened Coulomb potential and a delta function potential corresponding to the central-cell-correction (CCC). The CCC arises due to the differing chemical nature of various impurities. For our calculations  $V_c(\mathbf{r})$  is non-zero only on a single grid site, as shown in Fig. 1(b) along with the potential due to the applied electric field. The CCC is found by adjusting  $C$  until the calculated binding energy for the  $1s$  donor state matches experiment. The Landé  $g$  tensor for the impurity ground state was then obtained from the calculated Zeeman splitting of the  $1s$  level in a uniform magnetic field.

Fig. 2 shows  $g_{[001]}$ , the tensor component for the  $1s$  impurity state as a function of collinear magnetic and electric fields. Increasing the electric field increases the relative change in  $g$ , whereas increasing the magnetic field decreases the relative change in  $g$ . Appreciable changes in  $g$  are seen even at modest magnetic fields, which is encouraging for manipulating the donor atom's spin. The impurity  $g_{[001]}$ 's depend nonlinearly on the magnetic field, as shown in Fig. 2(b). This behavior is unlike that seen in small QDs such as treated in Ref. 17, for which the  $g$  tensor is nearly independent of the applied magnetic field.

The competing effects of  $B$  and  $E$  on  $g_{[001]}$  can be understood by examining the donor electron's wavefunction, shown in Fig. 3. As the magnetic field is increased in the  $[001]$  direction [from Fig. 3(a) to (b)], the cy-



**FIG. 2** Normalized donor  $g_{[001]}$  values as a function of (a)  $E_{[001]}$  and (b)  $B_{[001]}$ . Insets show unnormalized donor  $g_{[001]}$  values. The full range of the  $x$ -axis of the insets is the same as that of their respective (normalized) plots.



**FIG. 3** Calculated wavefunctions for (a)  $E_{[001]} = B_{[001]} = 0$ , (b)  $E_{[001]} = 0$ ,  $B_{[001]} = 4 \text{ T}$  (c)  $E_{[001]} = 0.15 \text{ mV/nm}$ ,  $B_{[001]} = 0$ . Contours outline selected amplitudes as a guide to the eye.

clotron radius decreases, contracting the extent of the wave function in the direction transverse to  $\mathbf{B}$ . Similarly, the opposite effect is evident when the electric field is increased [Fig. 3(c)], which allows the impurity wavefunction to spread into a region with lower overall potential. This decreases the confinement for the donor electron and thereby increases  $|g|$ [18]. This effect is more prominent for a smaller magnetic field.

The  $g$  tensor components were calculated for various directions of  $\mathbf{B}$  with  $\mathbf{E}$  applied along  $[001]$ , as shown in Fig. 4. Note that  $\partial g / \partial E$  decreases with increasing  $B$ . The variation in  $\partial g / \partial E$  as a function of  $B$  is greater when  $\mathbf{E} \perp \mathbf{B}$ . However at an intermediate  $B (\approx 2T)$ ,  $\partial g / \partial E$  is identical in all directions. These results imply that an electric field induces a  $g$  tensor anisotropy oriented relative to  $\mathbf{E}$ , which makes it possible to modulate the  $g$  tensor using an alternating electric field in addition to the static electric and magnetic fields.

We next solve for the donor atom's spin dynamics by explicitly integrating the time-dependent Schrödinger equation. The nonlinear nature of  $g$  complicates a *quantitative* treatment within the rotating-wave approximation. The directional dependence of  $g$  (Fig. 4) can be used to obtain an analytical form of the  $g$  tensor by fitting each

tensor component to the expression  $\sum_{n=0}^2 a_n(\mathbf{B}) E^{2n}$ . A time-dependent  $g$  tensor can then be constructed for the time-varying electric field  $E(t) = E_{dc} + E_{ac} \sin(\omega t)$ . The

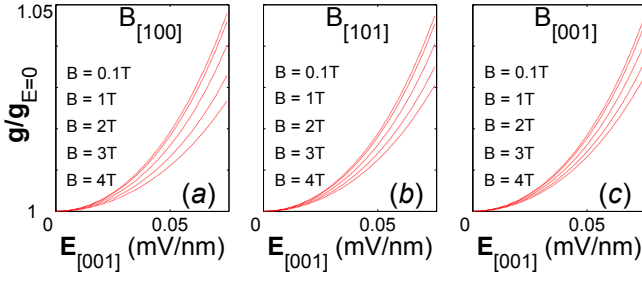


**FIG. 4**  $g$  as a function of  $E_{[001]}$  and  $B$  applied in various directions (a) [100] (b) [101] (c) [001].  $g$  is also calculated for various magnetic field strengths.

maximum amplitude of  $E(t)$  is always held constant at 0.2 mV/nm, so as not to exceed the breakdown field of the GaAs host. The spin dynamics of the donor atom can then be calculated using the effective time-dependent Hamiltonian,

$$H(t) = \frac{\mu_B}{2} \sigma \cdot \tilde{\mathbf{g}}(t) \cdot \mathbf{B} \quad (2)$$

where  $\mu_B$  is the Bohr magneton.

As the Hamiltonian is explicitly time dependent, the state of a spinor,  $S_j$  (where  $j = \downarrow, \uparrow$ ) at time  $t$  can be obtained by evolving  $S_j(t=0)$  forward in time in  $n$  steps of  $\Delta t = t/n \ll 1/2\omega$  as follows,

$$|S_j(t)\rangle = \hat{\mathbf{T}} \prod_{\nu=0}^n \exp\left(\frac{iH(t_\nu)\Delta t}{\hbar}\right) |S_j(0)\rangle \quad (3)$$

where  $\hat{\mathbf{T}}$  is the time-ordering operator. For sufficiently small  $\Delta t$  this is equivalent to

$$|S_j(t)\rangle = \hat{\mathbf{T}} \exp \int_0^t \left(\frac{iH(t')dt'}{\hbar}\right) |S_j(0)\rangle, \quad (4)$$

The time dependent probability of making a spin-flip transition is  $|\langle S_\uparrow(0)|S_\downarrow(t)\rangle|^2$ . Rabi oscillations are obtained when spin flip transitions are made resonantly (*i.e.*  $|\langle S_\uparrow(0)|S_\downarrow(t)\rangle|_{\max}^2 = 1$ ). Resonant spin flip transitions are usually made when  $E(t)$  is driven at the Larmor frequency  $\Omega_L$ . However in case of the hydrogenic impurity system considered here, the donor electrons spin can be resonantly flipped at any sub-harmonic of the Larmor frequency:  $\Omega_L/N$ , where  $N$  is an integer. This is illustrated in Fig. 5(a), where the peak spin-flip transition probabilities are shown as a function of the driving  $E$ -field frequency  $\omega$ . Multiple resonance lines are apparent, located at  $\Omega_L$  and its sub-harmonics. This unusual behavior arises from the highly nonlinear dependence of  $g$  on the applied electric field (Fig. 4). For sub-harmonics higher than  $N=2$ , the Rabi frequencies  $\Omega_R$  are lower than those at  $N < 2$  and hence are not considered further for spin manipulation. The largest  $\Omega_R$  can be achieved by driving  $E$  at the second sub-harmonic ( $N = 2$ ) of  $\Omega_L$ .

Due to the smaller DC component of the electric field the Rabi oscillations are less rapid at  $\Omega_L$ , than at its second sub-harmonic. The resonance lines in Fig. 5(a) at  $\omega = \Omega_L/N$ , have a full width at half maximum of  $\Delta\omega = 2\Omega_R/N$ .

The Rabi frequencies are calculated next as a function of  $E_{dc}$  and  $\theta$  and are shown in Fig. 5(b) with the electric field driven at  $\Omega_L$ . For all  $\theta$ , and  $\omega = \Omega_L$ ,  $\Omega_R$  is largest when the AC and DC components of the electric field are equal. If the electric field is driven at  $\Omega_L/2$ , however, as shown in Fig. 5(c), then  $\Omega_R$  is largest if  $E_{dc} = 0$ . In both Figs. 5(b) and (c), the optimal angle of the magnetic field to the electric field is  $\theta = 45^\circ$ . Although the maximum  $\Omega_R$  in Figs. 5(b) and (c) are identical, driving  $E$  at  $\Omega_L/2$  offers two key advantages. When the peak value of  $E$  is close to the breakdown of the host crystal, a pure AC field with an adjustable duty-cycle is much less likely to ionize the donor electron, as the carriers can recover during a thermal relaxation time. This allows for higher driving fields, which result in higher  $\Omega_R$ . It also may be experimentally more feasible to resonantly flip the spin at the lower frequency of the subharmonic  $\Omega_L/2$  than the fundamental  $\Omega_L$ .

Fig. 5(d) shows  $\Omega_R$  as a function of  $B$  for  $\theta = 45^\circ$

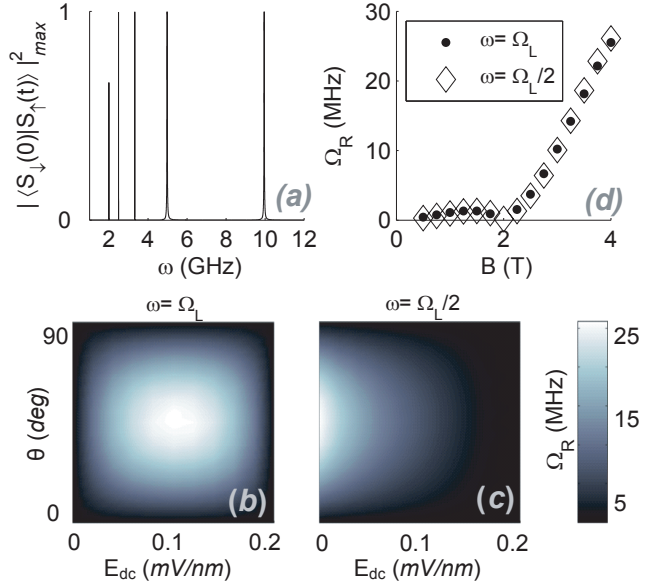


**FIG. 5** Spin dynamics of the donor atom as a function of various parameters.  $E_{ac} + E_{dc} = 0.2$  mV/nm and is [001] oriented.  $\theta$  is the angle between  $\mathbf{B}$  and  $\mathbf{E}$ . (a) Peak spin-flip transition amplitudes as a function of  $E$ 's driving frequency, for  $E_{ac}/E_{dc} = 9$  and  $\theta = 45^\circ$ . Resonant transitions appear at sub-harmonics of the Larmor frequency  $\Omega_L$ . (bc) Rabi frequency  $\Omega_R$  as a function of  $E_{dc}$  and  $\theta$  for: (b)  $E$  driven at  $\Omega_L$ ,  $\Omega_R$  is maximum at  $\theta = 45^\circ$  and  $E_{dc} = 0.1$  mV/nm. (c)  $E$  driven at  $\Omega_L/2$ ,  $\Omega_R$  is maximum at  $\theta = 45^\circ$  and  $E_{dc} = 0$ . (d)  $\Omega_R$  as a function of  $B$  for optimal  $\theta$  and  $E_{dc}$  of (b) and (c). Note that above  $B = 2T$ ,  $\Omega_R$  increases monotonically.

and  $E$  driven at  $\Omega_L$  or  $\Omega_L/2$ . For magnetic fields greater than  $2T$ ,  $\Omega_R$  increases monotonically, whereas below  $2T$   $\Omega_R$  exhibits a non-monotonic behavior. This feature can be explained by Taylor-expanding the time-dependent Hamiltonian to first order in the rotating wave approximation,

$$H(E) \approx \frac{\mu_B \sigma}{2} \cdot \left( \tilde{\mathbf{g}} + \frac{E_{ac}}{2} \frac{\partial \tilde{\mathbf{g}}}{\partial E} \Big|_{E=E_{dc}} \right) \cdot \mathbf{B}. \quad (5)$$

Here the Larmor frequency is given by the time independent static precession vector,  $\mathbf{\Omega}_0 = \mu_B \tilde{\mathbf{g}} \cdot \mathbf{B} / \hbar$  and the electron's spin dynamics in the rotating frame is described by the time-dependent spin precession vector,  $\mathbf{\Omega}_1(t) = \mu_B E_{ac} (\partial \tilde{\mathbf{g}} / \partial E) \cdot \mathbf{B} / 2\hbar$ .  $\mathbf{\Omega}_1$  can be resolved into components that are parallel ( $\mathbf{\Omega}_{||}$ ) and perpendicular ( $\mathbf{\Omega}_{\perp}$ ) to  $\mathbf{\Omega}_0$ . In the rotating frame,  $|\mathbf{\Omega}_{\perp}|$  is equivalent to  $\Omega_R$  (in the lab frame), as driving  $E$  at  $|\mathbf{\Omega}_0|$  leads to spin precession about  $\mathbf{\Omega}_{\perp}$  or Rabi oscillations. As the tensor components  $\partial g / \partial E$  decrease with increasing  $B$  (see Fig. 4), the magnitudes of  $B$  and  $\partial g / \partial E$  have opposing effects on  $\Omega_1$  (and hence  $\Omega_{\perp}$ ). For  $B < 1T$  the contribution from  $\partial g / \partial E$  dominates over  $B$  and hence the Rabi frequencies increase. For  $1T < B < 2T$  the competing contributions of  $B$  and  $\partial g / \partial E$  make the  $g$  tensor increasingly isotropic and the Rabi frequencies smaller. At  $B \approx 2T$  the  $g$  tensor becomes isotropic and the Rabi frequency vanishes. Above  $B \approx 2T$ , the effects of a much larger magnetic field dominate and the spin flip times decrease monotonically. Two key inferences, consistent with other work on  $g$ -TMR, can be drawn from this behavior. For spintronic applications the highest magnetic field possible is desirable in order to generate the largest possible Rabi frequencies. Secondly, the amount of  $g$ -tensor anisotropy induced is crucial to achieving shorter spin-flip times, not the degree of change in  $g$  as a function of  $E$ .

We have proposed a scheme for achieving electric-field driven  $g$ -tensor modulation resonance for a single shallow donor impurity. Electric and magnetic field dependent  $g$  tensors were calculated for the  $\text{Si}_{\text{Ga}}$  donor using 8-band  $\mathbf{k} \cdot \mathbf{p}$  theory on a real space grid. Varying  $\mathbf{E}$  and  $\mathbf{B}$  affects the confinement for the donor electron, which in turn alters its  $g$  tensor. In addition to the nonlinear  $E$  dependence, the  $g$  tensors are also highly nonlinear as a function of  $B$ . This is unlike the case for a QD, where  $g$  is essentially independent of  $B$ . A consequence of the nonlinear dependence of  $g$  on  $E$  is that spin-flip transitions can be made resonantly at any sub-harmonic of the Larmor frequency. Spin flip times were calculated exactly, using time evolution operators, and optimized for various parameters of interest. If  $E$  is driven at the second sub-harmonic of the Larmor frequency, then high

frequency Rabi oscillations can be obtained without any DC component of  $E$ . This could be particularly useful in obtaining the largest Rabi frequencies for a given breakdown-field limit for the semiconductor host.

C.E.P. would like to acknowledge a NSF NIRT. M.E.F. would like to acknowledge an ONR MURI.

- 
- [1] D. D. Awschalom, N. Samarth, and D. Loss, eds., *Semiconductor Spintronics and Quantum Computation* (Springer Verlag, Heidelberg, 2002).
  - [2] D. D. Awschalom and M. E. Flatté, *Nature Physics* **3**, 153 (2007).
  - [3] J. Levy, *Phys. Rev. Lett.* **92**, 147902 (2002).
  - [4] J.-M. Tang, J. Levy, and M. E. Flatté, *Phys. Rev. Lett.* **97**, 106803 (2006).
  - [5] T. Shinada, S. Okamoto, T. Kobayashi, and I. Ohdomari, *Nature* **437**, 1128 (2005).
  - [6] S. R. Schofield, N. J. Curson, M. Y. Simmons, F. J. Rueß, T. Hallam, L. Oberbeck, and R. G. Clark, *Phys. Rev. Lett.* **91**, 136104 (2003).
  - [7] D. Kitchen et al., *Nature* **442**, 436 (2006).
  - [8] D. Loss and D. P. DiVincenzo, *Phys. Rev. A* **57**, 120 (1998).
  - [9] B. E. Kane, *Nature* **393**, 133 (1998).
  - [10] H. W. Jiang and E. Yablonovitch, *Phys. Rev. B* **64**, 041307 (2001).
  - [11] T. Nakaoka, S. Tarucha, and Y. Arakawa, *Phys. Rev. B* **76**, 041301 (2007).
  - [12] Y. Tokura, W. G. van der Wiel, T. Obata, and S. Tarucha, *Phys. Rev. Lett.* **96**, 047202 (2006).
  - [13] J. R. Petta, A. C. Johnson, J. M. Taylor, E. A. Laird, A. Yacoby, M. D. Lukin, C. M. Marcus, M. P. Hanson, and A. C. Gossard, *Science* **309**, 2180 (2005).
  - [14] E. I. Rashba and A. L. Efros, *Phys. Rev. Lett.* **91**, 126405 (2003).
  - [15] K. C. Nowack, F. H. L. Koppens, Y. V. Nazarov, and L. M. K. Vandersypen, *Science* **318**, 1430 (2007).
  - [16] Y. Kato, R. C. Myers, A. C. Gossard, J. Levy, and D. D. Awschalom, *Science* **299**, 1201 (2003).
  - [17] J. Pingenot, C. E. Pryor, and M. E. Flatté, *Appl. Phys. Lett.* **92**, 222502 (2008).
  - [18] C. E. Pryor and M. E. Flatté, *Phys. Rev. Lett.* **96**, 026804 (2006); C. E. Pryor and M. E. Flatté, *Phys. Rev. Lett.* **99**, 179901(E) (2007).
  - [19] W. Kohn and J. M. Luttinger, *Phys. Rev.* **97**, 1721 (1955).
  - [20] L. M. Roth, B. Lax, and S. Zwerdling, *Phys. Rev.* **114**, 90 (1959).
  - [21] T. B. Bahder, *Phys. Rev. B* **41**, 11992 (1990).
  - [22] C. Pryor, *Phys. Rev. B* **44**, 12912 (1991).
  - [23] C. Pryor, *Phys. Rev. B* **57**, 7190 (1998).
  - [24] C. Pryor, M.-E. Pistol, and L. Samuelson, *Phys. Rev. B* **56**, 10404 (1997).
  - [25] I. Vurgaftman, J. R. Meyer, and L. R. Ram-Mohan, *J. Appl. Phys.* **89**, 5815 (2001).